Scilight

Low-Dimensional Materials

https://www.sciltp.com/journals/ldm

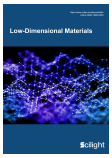

Supplementary Materials

A Synergistic Strategy through Microstructuring and Graphene Doping for High-Output Silk Fibroin-Based Triboelectric Nanogenerators toward Self-Powered Systems

Baizheng Zhu [1,†], Shiqi Zhang [1,†], Aoxiong He [1], Meng Sun [1], Qiaolin Fan [1], Zhonghua Ni [1,2], Xiao Li [1,2,*] and Tao Hu [1,2,*]

[1] School of Mechanical Engineering, Jiangsu Key Laboratory for Design and Manufacturing of Precision Medicine Equipment, Southeast University, Nanjing 211189, China
[2] Advanced Ocean Institute of Southeast University, Nantong 226010, China
* Correspondence: lx2016@seu.edu.cn (X.L.); hutao@seu.edu.cn (T.H.)
† These authors contributed equally to this work.

How To Cite: Zhu, B.; Zhang, S.; He, A.; et al. A Synergistic Strategy through Microstructuring and Graphene Doping for High-Output Silk Fibroin-Based Triboelectric Nanogenerators toward Self-Powered Systems. *Low-Dimensional Materials* **2025**, *1*(1), 5.

S1: Working Principles of Triboelectric Nanogenerators (TENGs)

When a TENG operates under external mechanical excitation, its output performance is typically characterized by open-circuit voltage (V_{oc}) and short-circuit current (I_{sc}). Under normal conditions, the two triboelectric electrodes remain electrically insulated. Due to the difference in work functions between the two triboelectric layers, contact and friction between them induce the generation of equal but opposite charges on their surfaces. These triboelectric charges establish a potential difference that drives current flow in the external circuit.

The operational principle of TENGs originates from Maxwell's equations, particularly the Maxwell-Ampere law, expressed as follows:

$$\nabla \times H = J_f + \frac{\partial D}{\partial t} \tag{S1}$$

The term J_f in Equation (S1) is defined as the Maxwell displacement current density. Unlike conductive electron current, displacement current arises from time-varying electric fields and the microscopic motion of bound charges, driven by dielectric polarization in materials [1]. When the electric field intensity E varies with time, it generates a time-dependent electric displacement field D in space. Their relationship is given by the following equation, where ε_0 denotes the vacuum permittivity and P represents the polarization field induced by surface static charges:

$$D = \varepsilon_0 E + P \tag{S2}$$

When two dissimilar materials come into contact and undergo friction, charge transfer occurs from the material with lower electron affinity to the one with higher electron affinity due to differences in their electronic potentials. This charge redistribution leads to the formation of static charges on the material surfaces. The accumulation of static charges directly influences the dielectric polarization of the materials, i.e., the separation of positive and negative charge centers within the material. In isotropic dielectrics, the polarization density induced by surface static charges and the resulting displacement current are expressed in Equation (S3). The dynamic variation of polarization in TENGs is the key mechanism for electrical energy generation.

$$J_D = \frac{\partial D}{\partial t} = \varepsilon_0 \frac{\partial E}{\partial t} + \frac{\partial P}{\partial t} \tag{S3}$$

When the respective back electrodes are connected to an external circuit, these charges form conductive pathways under the influence of the electric field. The voltage and current generated by TENGs typically manifest as pulsed signals, with each friction event producing a corresponding pulse. Furthermore, the open-circuit voltage

exhibits a linear relationship with the separation distance between the two electrodes. To maximize charge transfer efficiency, the minimum separation distance should be minimized, ideally approaching zero. In contrast, the short-circuit current is influenced by the effective contact area of the electrodes and the operational frequency. An increase in contact area or working frequency significantly enhances the short-circuit current.

$$\mathrm{V} = -\frac{Q}{S_{\varepsilon_0}}\left[\frac{d_1}{\varepsilon_{r_1}} + \frac{d_2}{\varepsilon_{r_2}} + x(t)\right] + \frac{\sigma x(t)}{\varepsilon_0} \tag{S4}$$

$$I_{sc} = \frac{dQ_{SC}}{dt} = \frac{S\sigma}{\left[\frac{d_1}{\varepsilon_{r_1}} + \frac{d_2}{\varepsilon_{r_2}} + x(t)\right]^2}\frac{dx}{dt} = \frac{S\sigma\left(\frac{d_1}{\varepsilon_{r_1}} + \frac{d_2}{\varepsilon_{r_2}}\right)v(t)}{\left[\frac{d_1}{\varepsilon_{r_1}} + \frac{d_2}{\varepsilon_{r_2}} + x(t)\right]^2} \tag{S5}$$

The expressions for open-circuit voltage and short-circuit current are given in Equations (S4) and (S5), respectively, where Q denotes the transferred charge quantity, S represents the effective contact area, d_1 and d_2 are the thicknesses of the two triboelectric layers, ε_{r_1}, ε_{r_2}, and ε_0 are the relative permittivities of the two triboelectric layers and air, $x(t)$ is the separation distance between the opposing surfaces of the triboelectric layers, and σ is the surface charge density upon contact [2–4].

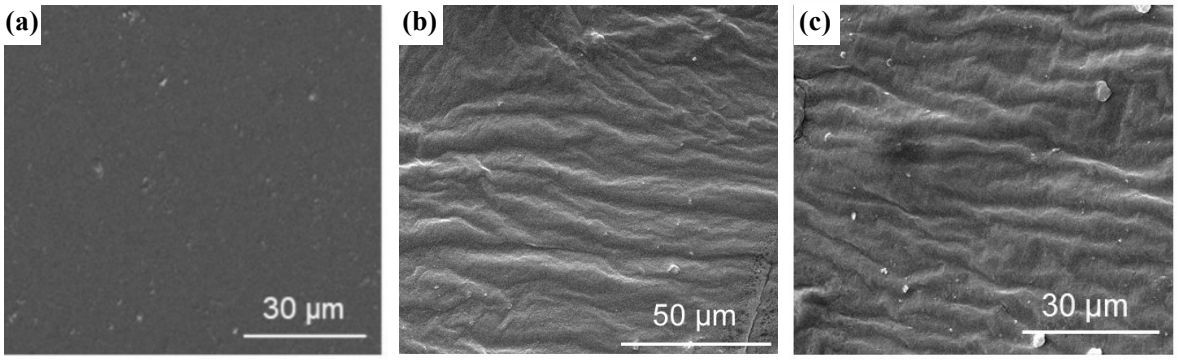

Figure S1. (**a**) SEM image of the surface of SF film; (**b**) SEM image of the cross-section of the SF film; (**c**) SEM image of the cross-section of the SF/graphene composite film.

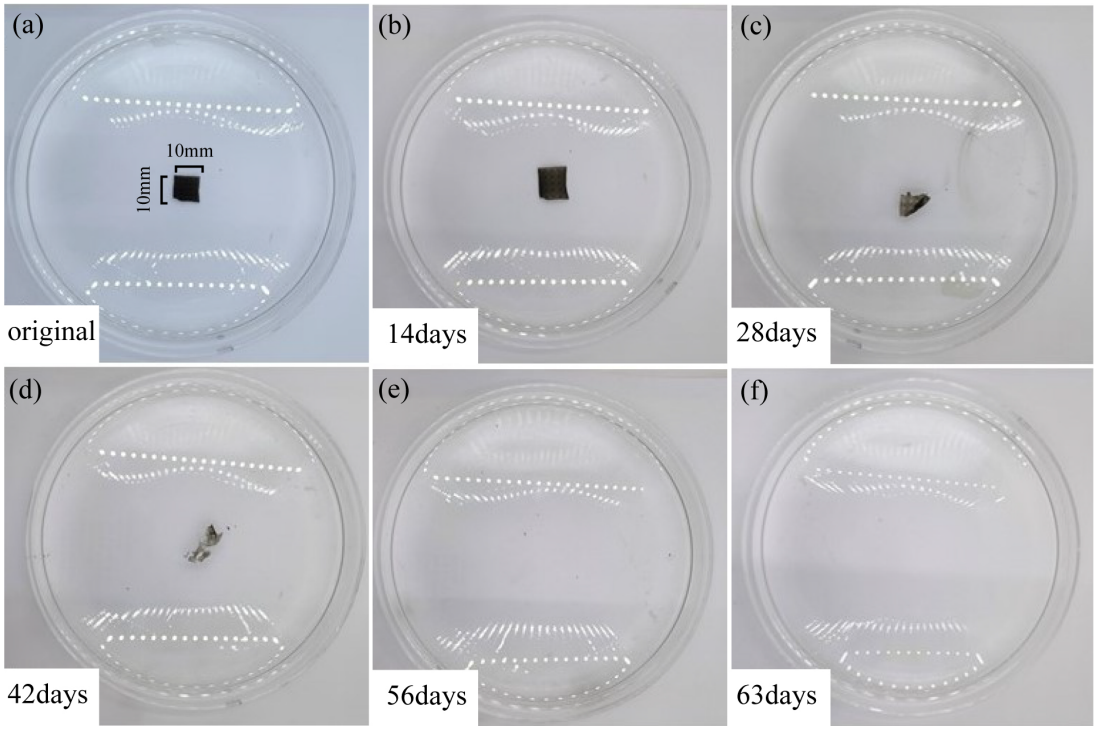

Figure S2. (**a**–**f**) Degradation test of silk fibroin/graphene composite films using deionized water for 63 days.

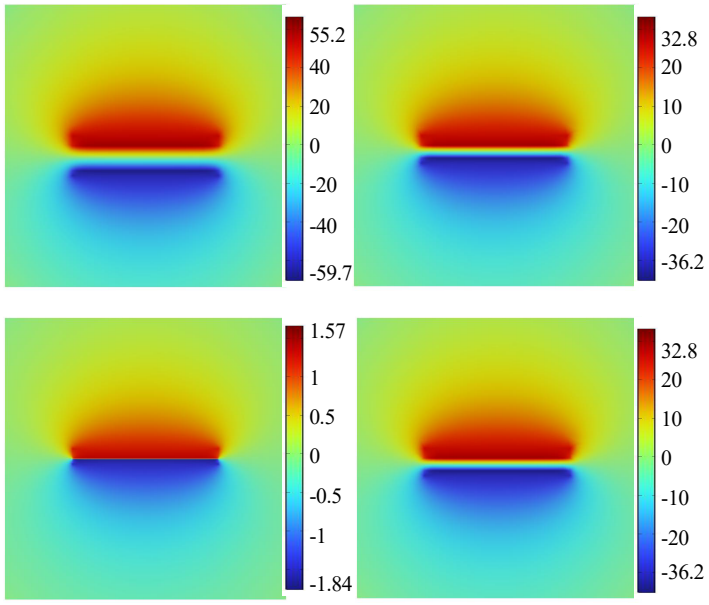

Figure S3. Electric potential distribution of the SF-PTFE TENG without microstructure obtained from simulation.

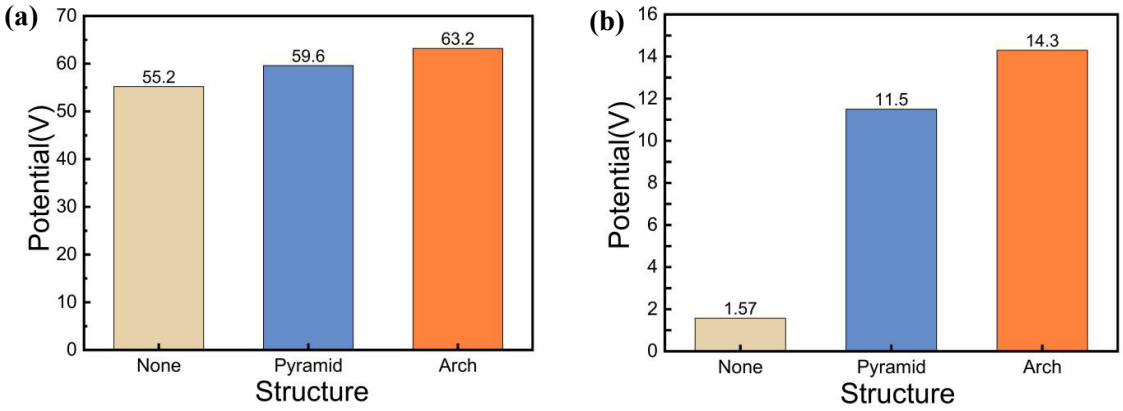

Figure S4. The maximum electric potential of TENG with different structures during (**a**) Separation and (**b**) Contact.

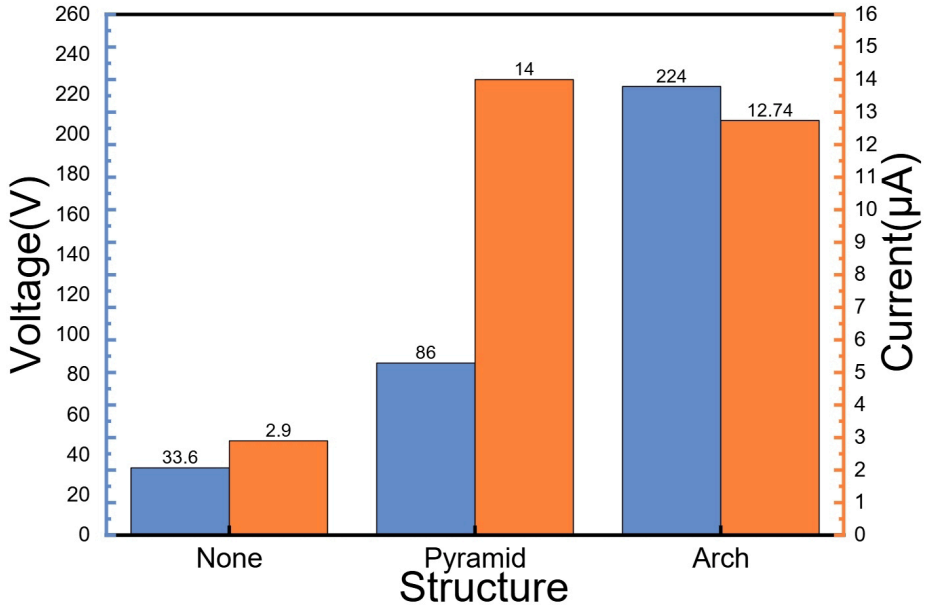

Figure S5. Comparison bar diagram of maximum peak-to-peak open-circuit voltage and short-circuit current for different microstructures with the density of 25 units/cm^2.

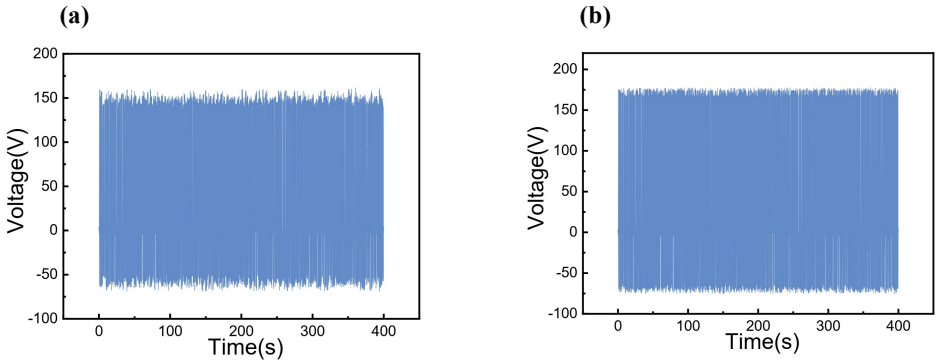

Figure S6. (**a**) Durability test of SF-PTFE TENG at a frequency of 2 Hz for 400 s; (**b**) Durability test of SF/graphene-PTFE TENG with a concentration of 0.5 mg at a frequency of 2 Hz for 400 s.

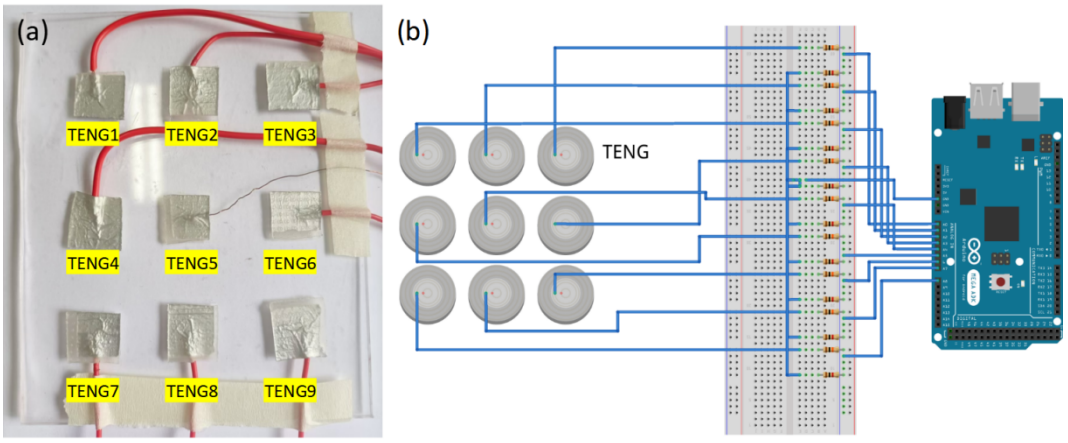

Figure S7. (**a**) Photograph of nine-grid format TENG recognition device; (**b**) Circuit diagram of the device connected to Arduino Mega2560.

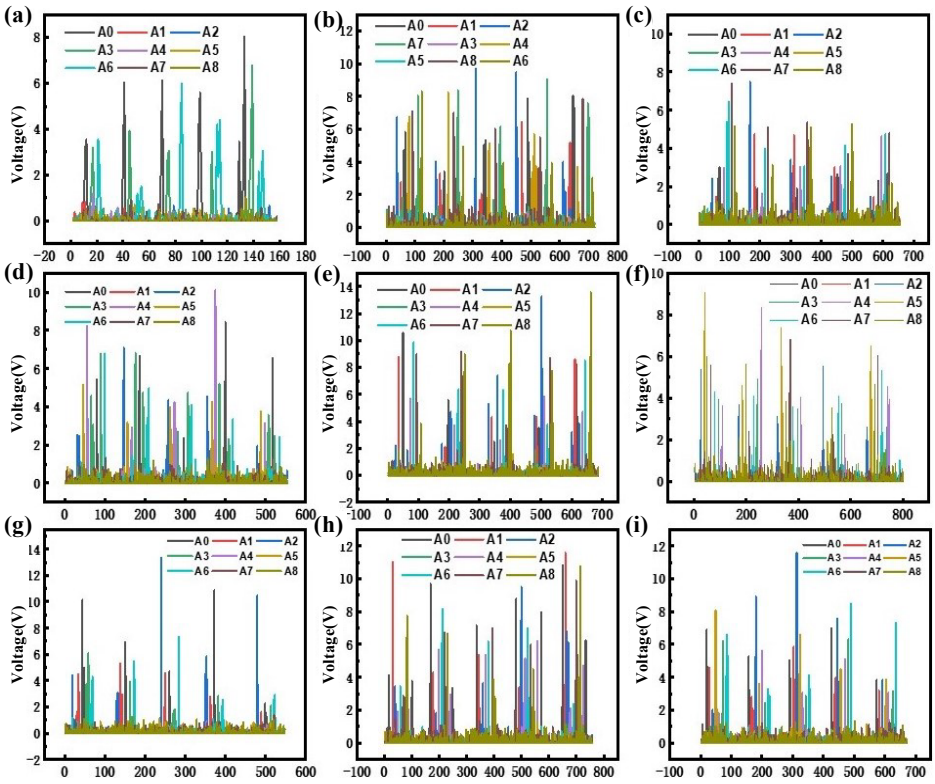

Figure S8. (**a**–**i**) Identification of device voltages for numbers 1 to 9.

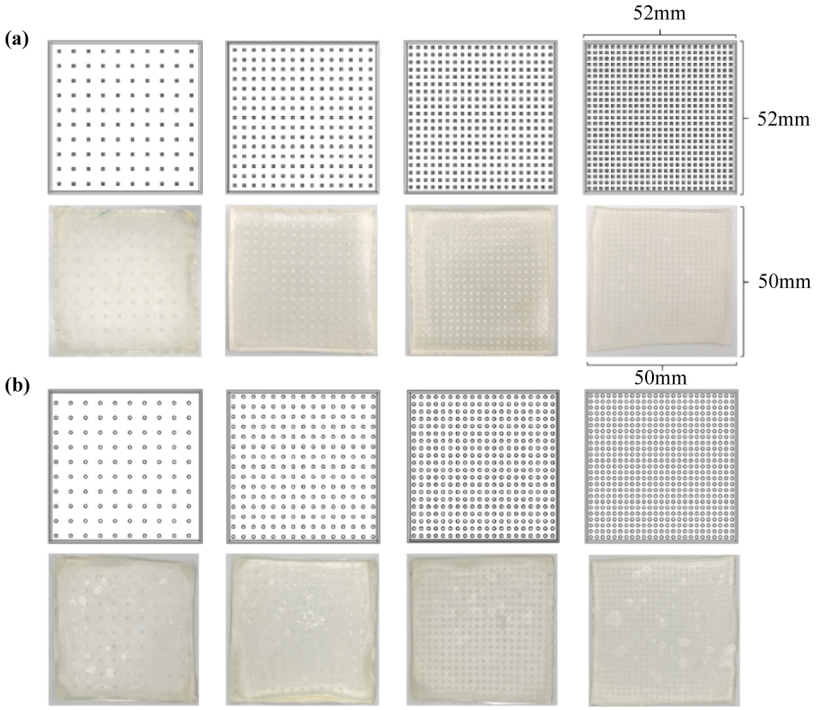

Figure S9. (**a**) Uniform array of micro-pyramid structures with different densities of silk protein films; (**b**) Uniform array of micro-arch structures with different densities of silk protein films.

Table S1. Comprehensive comparison of TENG output performance under different optimization conditions.

TENG Configuration	Microstructure Density (Units/cm²)	rGO Concentration (mg)	Operating Frequency (Hz)	Peak-to-Peak Open-Circuit Voltage (V)	Peak-to-Peak Short-Circuit Current (μA)
Flat SF Film	0	0	2	33.06	2.90
SF Film with Micro-Pyramid Array	4	0	2	51.60	10.22
	9	0	2	60.53	11.62
	16	0	2	72.19	12.50
	25	0	2	86.20	13.73
SF Film with Micro-Arch Array	4	0	2	111.94	4.04
	9	0	2	150.04	6.09
	16	0	2	196.13	8.80
	25	0	2	224.00	12.74
SF/Graphene Composite	25	0	2	224.00	12.74
		0.25	2	236.50	13.60
		0.50	2	267.24	16.59
		0.75	2	274.00	17.80
		1	2	288.60	20.06
		0.5	1	238.80	9.80
		0.5	2	267.24	16.59
		0.5	3	281.58	21.40
		0.5	4	306.16	28.20
		0.5	5	318.40	31.60

References

1. Wang, Z.L. On Maxwell's Displacement Current for Energy and Sensors: The Origin of Nanogenerators. *Mater. Today* **2017**, *20*, 74–82.
2. Niu, S.; Wang, S.; Lin, L.; et al. Theoretical Study of Contact-Mode Triboelectric Nanogenerators as an Effective Power Source. *Energy Environ. Sci.* **2013**, *6*, 3576–3583.
3. Niu, S.; Liu, Y.; Chen, X.; et al. Theory of Freestanding Triboelectric-Layer-Based Nanogenerators. *Nano Energy* **2015**, *12*, 760–774.
4. Niu, S.; Liu, Y.; Zhou, Y.S.; et al. Optimization of Triboelectric Nanogenerator Charging Systems for Efficient Energy Harvesting and Storage. *IEEE Trans. Electron Devices* **2015**, *62*, 641–647.